Analysis of Transport Phenomena in Cellulose Diacetate Membranes. I. Relation Between Dialysis Coefficients and Membrane Morphology and Hydration*

J. L. HALARY, C. NOËL, and L. MONNERIE, *Laboratoire de Physicochimie Structurale et Macromoléculaire, École Supérieure de Physique et de Chimie Industrielles de la Ville de Paris 10, Rue Vauquelin, 75231 Paris Cedex 05, France*

Synopsis

Transport properties were determined for various Loeb-type membranes which exhibit strong structure differences from one to another. Using linear relations of thermodynamics of irreversible processes for the homogeneous ones, correlations were found between the specific transport coefficients and the states of water in the membrane medium. In the case of heterogeneous membranes a schematic multilayer model, using in an appropriate way Darcy's law, was worked out in accordance with electron micrographs of membrane cross sections. It enables us to correlate the membrane hydraulic permeability with the relative extent of four typical structures A, B, C, and D. In addition, this model provides both the hydraulic specific permeabilities of these types of structure and their hydration characteristics.

INTRODUCTION

Studies[1] have been carried out on the physicochemical processes occurring during the acetone evaporation from films obtained by casting solutions consisting of 22.20 g cellulose diacetate, 66.70 g acetone, 10.00 g water, and sometimes 1.10 g of an anhydrous inorganic salt. Three successive regimes of evaporation have been identified, the first two ending at critical times t_1 and t_2, respectively. Quantitative data concerning the conditions of phase separation within casting solutions have shown that t_1 corresponds to the period of evaporation required to bring about polymer precipitation at the film surface and that time t_2 characterizes the complete gelation of the medium.

Furthermore, recent studies[2] of the interaction of water with cellulose acetate (CA) membranes have been carried out and the relative amounts of freezing (capillary) and nonfreezing (bound) water have been determined, using dehydration and differential scanning calorimetry measurements. It has been shown that the amount of bound water varies depending whether the CA precipitation results from water penetration into the cast film in the leaching bath or from solvent evaporation during the evaporation period. Finally, the structures of these membranes have been elucidated with the aid of scanning and transmission electron microscopy.[2,3] A three-layer morphological model has been discussed in relation to the evaporation time during the casting step. Results relevant to

*Paper presented in part at the 26th International Congress I.U.P.A.C., held in Tokyo, Japan, September 4–10, 1977.

Journal of Applied Polymer Science, Vol. 24, 985–998 (1979)

0021-8995/79/0024-0985$01.00

casting solutions containing $Mg(ClO_4)_2$ and KSCN as inorganic salt are shown in Figure 1.

The purpose of the present work is to correlate some transport properties, such as specific phenomenological coefficients of homogeneous membranes and hydraulic permeability of multilayer membranes, with these previously determined membrane characteristics.

EXPERIMENTAL

Membrane Preparation

According to the procedure developed by Loeb and Sourirajan,[4] composition of the casting solution, in weight percent, was as follows: Eastman–Kodak cellulose diacetate (E 398-3), 22.2; acetone, 66.7; water, 10.0; and anhydrous inorganic salt [$Mg(ClO_4)_2$ or KSCN], 1.1. The casting solution was uniformly spread at 2°C under an atmospheric relative humidity of 82% over a glass plate using a knife that is adjusted to obtain a film thickness of 0.15 mm. After a predetermined evaporation phase (2 to 2700 sec) at 2°C, the film was immersed in a water bath at 2°C for about 1 hr. Membranes obtained in this way were kept in distilled water before study. Hereafter, the membrane will be designated by one of the symbols MG or K according to the nature of the inorganic salt $Mg(ClO_4)_2$ or KSCN, respectively, with an additional number corresponding to the duration of the evaporation period.

Transport Coefficient Measurements

Apparatus. Experiments were carried out at 25.00 ± 0.01°C, using an apparatus especially designed for this purpose in our laboratory[5] (Fig. 2). This apparatus, supplied with two independent feedback mechanisms on both sides of

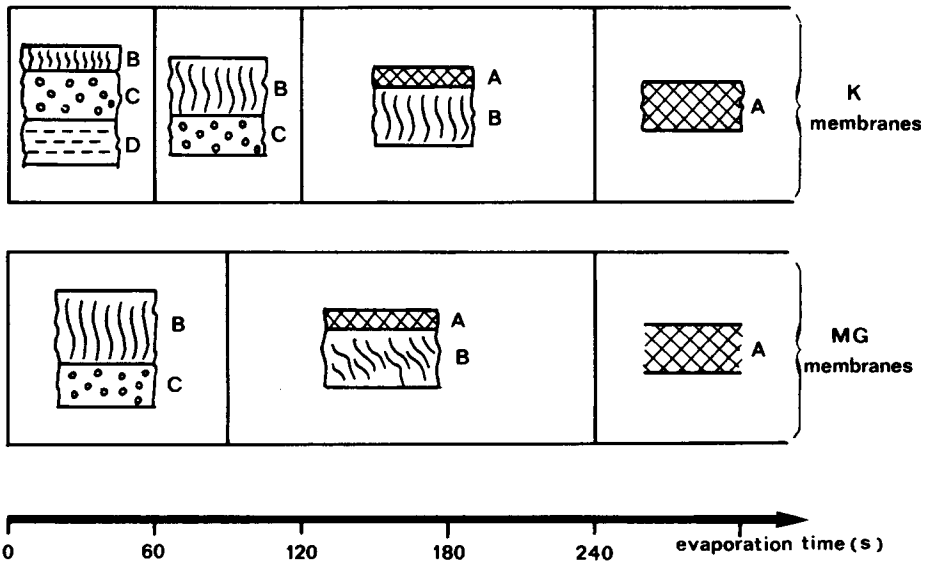

Fig. 1. Evolution of morphology of MG and K membranes as function of evaporation time, as evidenced by electron microscopy in references 2 and 3.

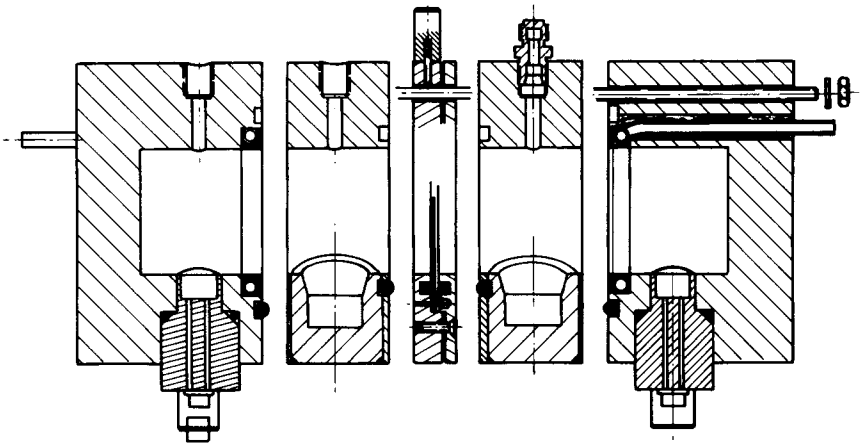

Fig. 2. Sectional drawing of the transport cell.

the membrane, is a modified version of the one previously built by Spiegler for the study of ionic membranes.[6] The membrane was held in the transport cell by two sheets of polyimide (Rhône–Poulenc Kerimid 601) which were 0.5 mm thick and had been drilled by 100 holes of 3 mm diameter brought into alignment (Fig. 3). The bulk solutions were stirred near both sides of the membrane by using two magnetic spin fins whose uniform rotation was monitored by two external magnets. The speed of rotation was chosen so that further increase in the speed did not modify any more the transport of salt and water across the membrane. The apparatus was designed for measuring (i) the changes in volume of each compartment, using calibrated capillaries, and (ii) the changes in electrical resistance of each solution using conductivity probes and impedance comparators.

Measurements. Measurements of transport coefficients were performed

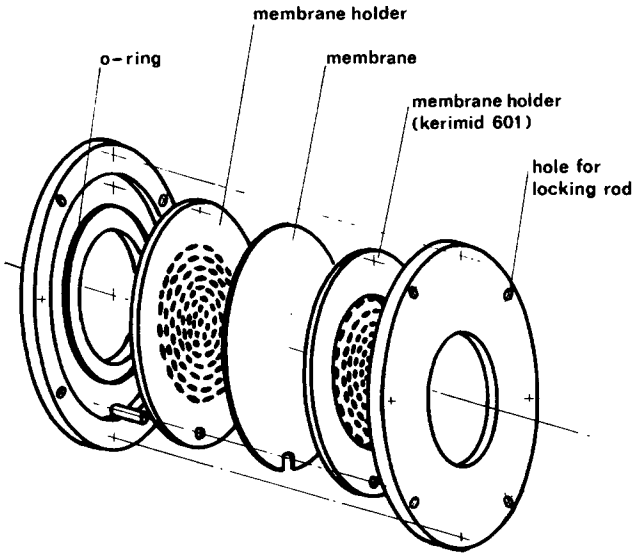

Fig. 3. Details of the membrane holder.

on aqueous solutions of sodium chloride adjusted to a molarity around 0.1. In most cases, five experiments were carried out for each membrane, under conditions of pressure and solute molarity schematized in Table I (experiments 1 to 5).

For the MG membranes, salt and water fluxes were measured by applying the higher pressure (i.e., P') either to the so-called AL side of the membrane, corresponding to the air-casting solution interface, or to the SU side of the membrane, corresponding to the glass plate–casting solution interface. In this case two independent sets of experiments were performed with two different samples of a same membrane.

Additional measurements were carried out in order to get information on the solute concentration dependence of transport coefficients, especially of the hydraulic permeability coefficient. Corresponding pressure and solute concentration conditions are given in Table I (experiments 6 to 12).

Reproducibility in Experimental Measurements. Several series of measurements were carried out on various membranes in order to check the reliability of results. The confidence range of the experimental data is rather large (up to 10%). This is largely due to the fact that it is difficult to get reproducible membranes in the wet process, even by fixing carefully all the casting variables. The origin of such a lack of reproducibility is in fact difficult to state.[7]

EXPERIMENTAL DATA PROCESSING

From the results of each experiment, the water flux J_W, the solute flux J_S, the total volume flux J_V, and the chemical flux J_D, which represents the apparent mean velocity of the solute relative to the water, were evaluated by a least-squares regression analysis.

Owing to the fact that the partial molar volumes of the water and the solute are nearly the same and that very small fractional change in pressure and composition occur during the measurements, one can rightfully, at least for homogeneous membranes, calculate[8] phenomenological coefficients from the fluxes given above, using the linear relations of nonequilibrium thermodynamics. Two

TABLE I
Experimental Conditions

Experiment No.	Higher pressure compartment		Higher salinity compartment	
	Pressure P', atm	NaCl concentration C', molarity	Pressure P'', atm	NaCl concentration C'', molarity
1	1.20	0.100	1.00	0.100
2	1.00	0.095	1.00	0.105
3	1.20	0.095	1.00	0.105
4	1.00	0.090	1.00	0.110
5	1.20	0.090	1.00	0.110
6	1.20	0.000	1.00	0.000
7	1.20	0.050	1.00	0.050
8	1.20	0.045	1.00	0.055
9	1.20	0.100	1.00	0.100
10	1.20	0.095	1.00	0.105
11	1.20	0.150	1.00	0.150
12	1.20	0.145	1.00	0.155

sets of equations can be used regarding the fluxes and forces under consideration. The first one describes the system in terms of fluxes of water J_W and solute J_S and chemical potentials of water and solute as their conjugate forces[9]:

$$J_W = L_W[\Delta(\mu_W + \overline{V}_W P)] + L_{WS}[\Delta(\mu_S + \overline{V}_S P)] \quad (1)$$

$$J_S = L_{SW}[\Delta(\mu_W + \overline{V}_W P)] + L_S[\Delta(\mu_S + \overline{V}_S P)] \quad (2)$$

These equations will be used subsequently in order to check the Onsager reciprocal relation between crossing coefficients, $L_{WS} = L_{SW}$.

The second formalism, which is obviously strictly equivalent, involves the volume flux J_V and the chemical flux J_D. The conjugate forces[10,11] are the pressure difference ΔP and the osmotic pressure difference $\Delta\pi$:

$$J_V = l_P \Delta P + l_{P\pi} \Delta\pi \quad (3)$$

$$J_D = l_{\pi P} \Delta P + l_\pi \Delta\pi \quad (4)$$

Though difficulties arise in practice to check that $l_{\pi P}$ equals $l_{P\pi}$, because of the large experimental errors affecting the $l_{\pi P}$ term, eqs. (3) and (4) will be mainly used in this paper (by assuming that $l_{\pi P} = l_{P\pi}$). Such a description in terms of coefficients l_P, $l_{P\pi}$, and l_π is in fact frequently used in the literature,[12,13] and in addition it permits introduction of the reflection coefficient σ, defined by Staverman[14] as $\sigma = -l_{P\pi}/l_P$.

RESULTS

Concerning the transport properties of MG membranes, all the details are given in Tables II, III, and IV.

Apart from the membrane MG 150, there is no significant difference for a given membrane between the values of phenomenological coefficients corresponding either to the position AL or SU (Tables II and III). Bearing in mind the well-known paper of Banks and Sharples[15] which demonstrates the directionality

TABLE II
Values of MG Membrane Thicknesses and Transport Coefficients l_P, $l_{P\pi}$, l_π, and σ

Membrane	Thickness,[2] μm	$10^4 l_P$, cm/sec-atm	$-10^5 l_{P\pi}$, cm/sec-atm	$10^4 l_\pi$, cm/sec-atm	σ
MG 2 AL	74	0.91	1.50	0.40	0.16
MG 30 AL	66	1.30	0.72	0.43	0.06
MG 30 SU		1.20	1.10	0.65	0.09
MG 60 AL	61	2.00	0.45	0.58	0.02
MG 60 SU		2.10	0.44	0.55	0.02
MG 90 AL	58	2.70	0.12	0.60	0.01
MG 90 SU		2.80	0.20	0.65	0.01
MG 120 AL	57	2.34	0.19	0.54	0.01
MG 150 AL	55	0.70	0.67	0.49	0.10
MG 150 SU		1.20	0.33	0.72	0.03
MG 240 AL	36	0.74	0.80	0.48	0.11
MG 240 SU		0.91	0.73	0.48	0.08
MG 480 AL	32	0.37	0.35	0.21	0.09
MG 480 SU		0.38	0.39	0.19	0.10
MG 1500 AL	28	0.29	—	—	—
MG 2700 AL	26	0.29	—	—	—

TABLE III
Values of Phenomenological Coefficients L_W, L_{WS}, L_{SW}, and L_S for MG Membranes

Membrane	Phenomenological coefficients, mole²/cm⁵-atm-sec			
	$10^6 L_W$	$10^9 L_{WS}$	$10^9 L_{SW}$	$10^{12} L_S$
MG 2 AL	0.28	0.45	0.42	1.20
MG 30 AL	0.40	0.64	0.59	1.40
MG 30 SU	0.38	0.63	0.70	2.20
MG 60 AL	0.60	1.00	1.10	2.70
MG 60 SU	0.70	1.20	1.30	3.60
MG 90 AL	0.80	1.60	1.60	3.80
MG 90 SU	0.87	2.50	2.80	4.00
MG 120 AL	0.69	1.50	1.46	3.60
MG 150 AL	0.22	0.29	0.30	0.73
MG 150 SU	0.37	0.52	0.58	1.30
MG 240 AL	0.23	0.39	0.39	1.30
MG 240 SU	0.26	0.49	0.34	0.77
MG 480 AL	0.12	0.20	0.19	0.48
MG 480 SU	0.11	0.17	0.16	0.46

TABLE IV
Solute Concentration Dependence of the Hydraulic Permeability Coefficient (cm/sec-atm) for MG Membranes

Membrane	Hydraulic permeability coefficient, cm/sec-atm			
	0 10^4 mole/cm³ [a]	0.5 10^4 mole/cm³	1.0 10^4 mole/cm³	1.5 10^4 mole/cm³
MG 60 AL	2.30		2.00	
MG 90 SU		2.80		2.70
MG 150 SU	1.20		1.20	
MG 240 AL	0.79	0.78	0.74	0.73

[a] Solute concentration.

of cellulose acetate membranes, one could consider this finding as surprising. However, directionality effects have been observed under high pressures (up to 100 atm), whereas our data refer to very low pressure difference (0.2 atm). Such a remark suggests that the membrane asymmetrical behavior, due to an accumulation of salt in the SU region, is magnified when pressure increases because of an increase in water removal. This phenomenon can be ignored under very low applied pressures, except for membranes which exhibit the largest differences in morphology between AL and SU regions (for example, membrane MG 150). In addition, Table III permits to check with a good accuracy the reciprocal relationship $L_{WS} = L_{SW}$ for all the membranes under study, in both AL and SU positions.

Finally, data on solute dependence of the hydraulic permeability are given in Table IV. As it can be seen on these examples, no significant variations in l_P values are detected over the concentration range 0–0.15 molar.

In the case of K membranes, similar conclusions can be drawn about (1) the nondirectionality under an applied pressure difference of 0.2 atm; (2) the check of the Onsager relation $L_{WS} = L_{SW}$; (3) the constancy of the hydraulic permeability, whatever the solute concentration up to 0.15 molar.

Therefore, Table V shows solely the values of the coefficients l_P, $l_{P\pi}$, l_π, and σ obtained from experiments carried out on the AL position.

RELATION BETWEEN TRANSPORT COEFFICIENTS AND MEMBRANE MORPHOLOGY AND HYDRATION

Since the use of eqs. (1) to (4) might be questionable in the case of heterogeneous membranes, we will consider independently the membranes prepared with an evaporation period shorter than 240 sec from the others which are homogeneous (Fig. 1).

Concerning the homogeneous membranes, one has to take in consideration the data relative to membranes MG 240, MG 480, MG 1500, MG 2700, K 240, K 330, and K 480, for which scanning electron micrographs of cross sections do not reveal any gradient of porosity, even at a magnification of 50,000.[16] However, the relevant values of the coefficients l_P, $l_{P\pi}$, and l_π cannot be compared because the membrane thicknesses are noticeably different (Tables II and V). Therefore, it is advisable to change these l_i coefficients into specific coefficients $\mathcal{L}_i$, defined as the product of l_i by the thickness of each membrane. The confrontation of the values of the specific transport coefficients with our previous measurements of capillary and bound water allows us to establish two original relationships: (i) between the values of $\mathcal{L}_P$ and $\mathcal{L}_\pi$ and the amount of capillary water per gram of dry cellulose acetate (Fig. 4), and (ii) between the absolute values of $\mathcal{L}_{P\pi}$ and the amount of bound water per gram of dry cellulose acetate (Fig. 5).

Such correlations between some macroscopic data and others at a molecular level bring a decisive contribution to the understanding of some transport phenomena such as the dependence of hyperfiltration membrane performance on applied pressure, as previously reported in preliminary notes.[17,18]

For all the other membranes under study in this paper, the morphological investigation previously carried out using scanning and transmission electron microscopy[2,3] has revealed dramatic evolutions of membrane structure which can be conveniently described by a model involving two or three layers of different structures, called A, B, C, and D (Fig. 1).

Nevertheless, since we have shown (Table IV) that l_P is independent of solute concentration and thus can be regarded as the membrane permeability coefficient in pure water conditions, one can discuss the values of l_P in Tables II and V in terms of Darcy's law. Using again specific coefficients, normalized with respect to layer thickness, we may write, according to Figure 6, for two-layer membranes,

$$J_{Wi} = \mathcal{L}_i(P_1 - P_2)/e_i = J_{Wj} = \mathcal{L}_j(P_2 - P_3)/e_j \qquad (5)$$

hence, after rearrangement into a symmetrical form,

TABLE V
Values of K Membrane Thicknesses and Transport Coefficients l_P, $l_{P\pi}$, l_π, and σ

Membrane	Thickness,[2] μm	$10^4\, l_P$, cm/sec-atm	$-10^5\, l_{P\pi}$, cm/sec-atm	$10^4\, l_\pi$, cm/sec-atm	σ
K 2	60	0.02	0.10	0.03	0.50
K 30	54	0.05_5	0.19	0.04_5	0.35
K 60	48	0.23	0.82	0.17	0.36
K 90	45	0.46	1.50	0.40	0.33
K 120	44	1.31	0.75	0.66	0.06
K 150	42	0.61	0.95	0.49	0.16
K 240	35	0.49	0.95	0.33	0.19
K 330	33	0.40	0.89	0.29	0.23
K 480	31	0.31	0.80	0.28	0.27

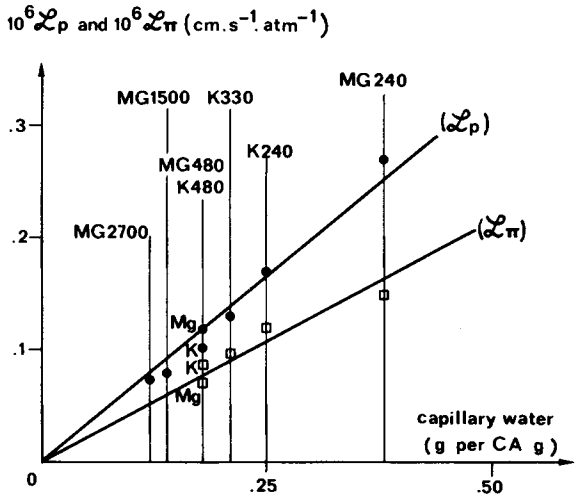

Fig. 4. Relationship between the $\mathcal{L}_P$ and $\mathcal{L}_\pi$ values and the capillary water content of homogeneous MG and K membranes.

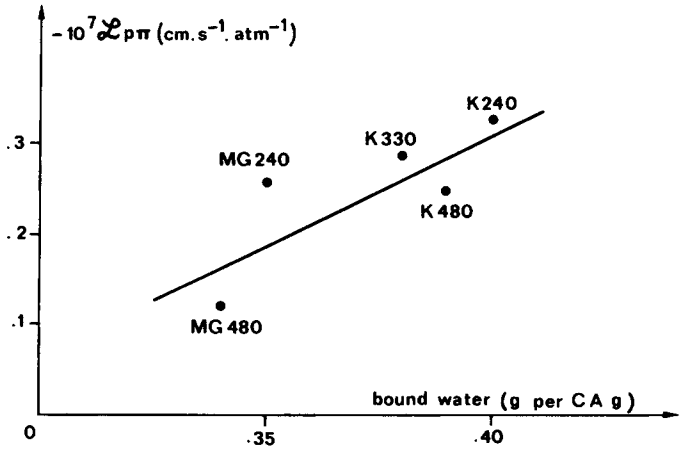

Fig. 5. Relationship between the absolute values of $\mathcal{L}_{P\pi}$ and the bound water content of homogeneous MG and K membranes.

$$(e_i\mathcal{L}_j + e_j\mathcal{L}_i)l_P = \mathcal{L}_i\mathcal{L}_j \tag{6}$$

and for three-layer membranes,

$$J_{Wi} = \frac{\mathcal{L}_i(P_1 - P_2)}{e_i} = J_{Wj} = \frac{\mathcal{L}_j(P_2 - P_3)}{e_j} = J_{wk} = \frac{\mathcal{L}_k(P_3 - P_4)}{e_k} \tag{7}$$

hence,

$$(e_i\mathcal{L}_j\mathcal{L}_k + e_j\mathcal{L}_i\mathcal{L}_k + e_k\mathcal{L}_i\mathcal{L}_j)l_P = \mathcal{L}_i\mathcal{L}_j\mathcal{L}_k \tag{8}$$

Equations (6) and (8) permit calculations of the specific hydraulic permeabilities $\mathcal{L}_{PA}$, $\mathcal{L}_{PB}$, $\mathcal{L}_{PC}$, and $\mathcal{L}_{PD}$ corresponding to structures A, B, C, and D, respectively, using some l_P values (Tables II and V) and layer thicknesses determined from electron micrographs of membrane cross sections.[2,3] These calculations are summarized in Table VI for both sets of K and MG membranes. They show essentially that the specific hydraulic permeability of the B-type structure is systematically higher than that of either the A or B type.

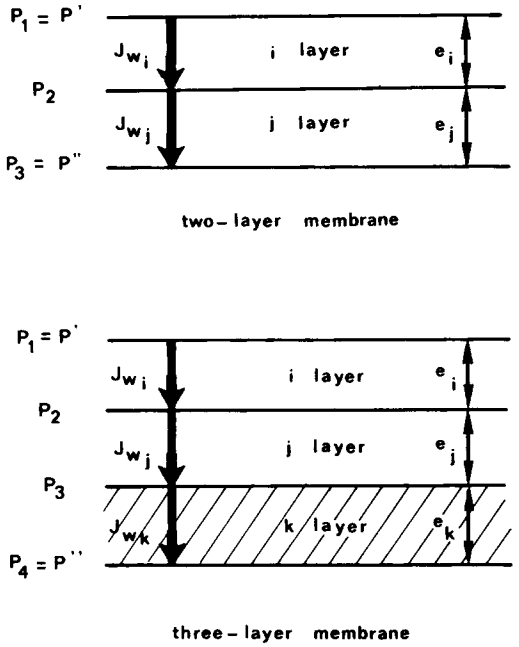

Fig. 6. Diagram of fluxes and pressures in accordance with Darcy's law for two and three layer membranes.

Equations (6) and (8) permit also evaluation of the different layer thicknesses for the membranes which were not used as a basis for the calculations given in Table VI. Such an evaluation is interesting in two separate ways. First, it is useful to check the validity of our schematic approach for some membranes whose micrographs yield accurate measurements of layer thicknesses. As shown in Table VII, the calculated thicknesses are very close to those measured by electron microscopy. In addition, such calculations provide further information concerning the membrane morphology when the differentiation between A, B, C, or D layers is hampered by a lack of contrast in electron micrographs (for example, K 150). They make it possible to outline the variations in the different layer relative thicknesses as a function of the evaporation time, as shown in Figures 7 and 8 for MG and K membranes, respectively. In the early stages of evaporation, these diagrams show an increase in the thickness of the B structure which is higher in MG membranes than in K membranes. In addition, they exhibit a slower advancement of the A-type structure extent for the MG system than for the K system. These two findings agree with the results given in a previous paper[19] which demonstrate that the swelling power is higher and the speed of gelation slower for the MG system than for the K system.

Taking advantage of the correlations between the l_P values and the morphological structure of multilayer membranes, we would like to reopen briefly the question of the validity of eqs (3) and (4) for describing the transport properties of such membranes. Over and above the check of the Onsager reciprocal relation between crossing coefficients L_{WS} and L_{SW} (Table II), two qualitative observations, which show the physical meaning of phenomenological coefficient values, seem to decide in favor of the suitability of such equations. First, for both MG and K systems, as shown in Tables II and V, respectively, the evolution of l_π

TABLE VI
Calculated Values of $\mathcal{L}_{PA}$, $\mathcal{L}_{PB}$, $\mathcal{L}_{PC}$, and $\mathcal{L}_{PD}$ from Data Corresponding to Both K and MG Membrane Systems

Membrane	Experimental data[a]	Layer specific permeability coefficient: Mode of calculation	Layer specific permeability coefficient: Calculated value, $cm^2/sec\text{-}atm$
K 240	l_P (Table V) $e_A = 35\ \mu m$ (Table V) l_P (Table V)	normalization	$\mathcal{L}_{PA}(K) = 0.17 \times 10^{-6}$
K 120	$e_A = 2\ \mu m$ $e_B = 42\ \mu m$ l_P (Table V)	eq. (6), using also $\mathcal{L}_{PA}$ value	$\mathcal{L}_{PB}(K) = 0.65 \times 10^{-6}$
K 60	$e_B = 15\ \mu m$ $e_C = 33\ \mu m$ l_P (Table V)	eq (6), using also $\mathcal{L}_{PB}$ value	$\mathcal{L}_{PC}(K) = 0.80 \times 10^{-7}$
K 2	$e_B = 3\ \mu m$ $e_C = 35\ \mu m$ $e_D = 22\ \mu m$	eq. (8), using also $\mathcal{L}_{PB}$ and $\mathcal{L}_{PC}$ values	$\mathcal{L}_{PD}(K) = 0.48 \times 10^{-8}$
MG 240	l_P (Table II) $e_A = 36\ \mu$ (Table II) l_P (Table II)	normalization	$\mathcal{L}_{PA}(MG) = 0.27 \times 10^{-6}$
MG 30	$e_B = 44\ \mu m$ $e_C = 22\ \mu m$ l_P (Table II)	eq. (6) yielding two independent relations	$\mathcal{L}_{PB}(MG) = 1.90 \times 10^{-6}$ $\mathcal{L}_{PB}(MG) = 0.41 \times 10^{-6}$
MG 2	$e_B = 37\ \mu m$ $e_C = 37\ \mu m$		

[a] Layer thicknesses were determined by electron microscopy.[2]

TABLE VII
Check Between Some Calculated Values of Layer Thicknesses and Corresponding Electron Microscopy Data

Membrane	Layer thicknesses, μm: Obtained from micrographs of membrane cross sections	Layer thicknesses, μm: Calculated using $\mathcal{L}_{PA}$, $\mathcal{L}_{PB}$, $\mathcal{L}_{PC}$ and $\mathcal{L}_{PD}$ values
K 30	$e_B = 7$ $e_C = 39$ $e_D = 8$	$e_B = 7$ $e_C = 41$ $e_D = 6$
K 90	$e_B \# 35$ $e_C \# 10$	$e_B = 32$ $e_C = 13$
MG 90	$e_B \# 56$ $e_C \# 2$	$e_B = 55$ $e_C = 3$
MG 150	$e_A > 15$ $e_B > 20$	$e_A = 17$ $e_B = 38$

values versus evaporation period is quite similar to those of l_P values, which have received a morphological explanation. Second, the combination of $l_{P\pi}$ values with unquestionable l_P values yields an evolution of the reflection coefficient σ (Tables II and V) which is similar to those of the rejection factor determined in hyperfiltration measurements.[17] In addition, the σ values lead to the following layer selectivity order (progressing from strong to weak selectivity): C type > A type $\gg$ B type, which agrees with other conclusions given in the literature.[20]

Finally, the results presented in Figures 7 and 8 can be compared with the data

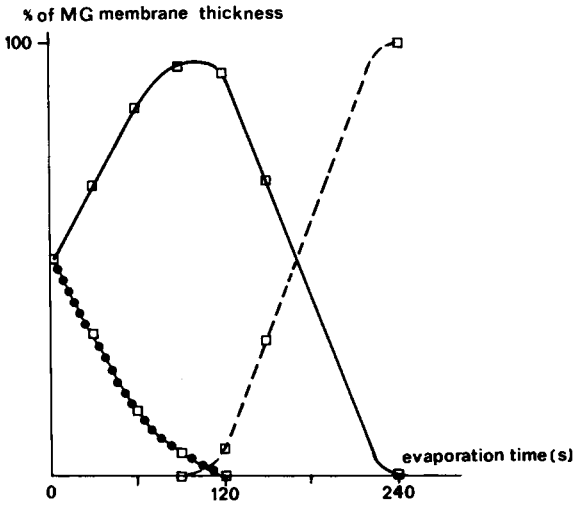

Fig. 7. Evolution of the relative thicknesses of A, B, and C type structures in MG membranes as function of evaporation time: (- - -) A structure; (—) B structure; (●—●) C structure.

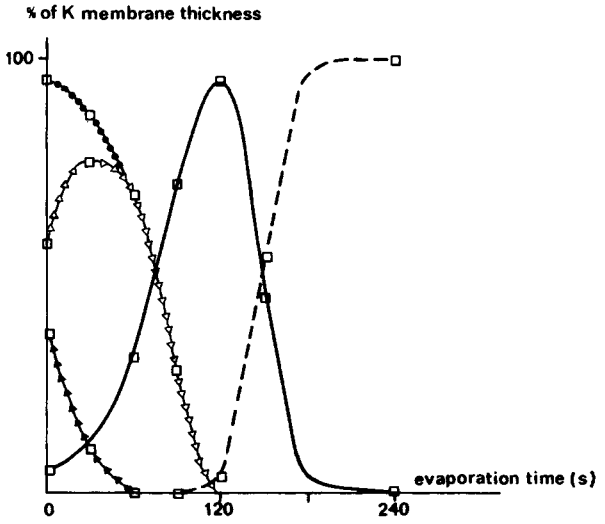

Fig. 8. Evolution of the relative thicknesses of A, B, C, and D type structures in K membranes as a function of evaporation time: (- - -) A structure; (—) B structure; (◁—◁) C structure; (◀—◀) D structure; (●—●) C + D.

given in reference 2 concerning the states of water in corresponding membranes, with intent to determine the hydration characteristics of the A, B, C, and D structures. For this purpose let us calculate the free water content FWC of the membrane K 150. According to the morphological model α, the FWC of the membrane K 240 is assumed to be characteristic of an homogeneous membrane of the A structure. Then, in its simplest form, the relationship between a, the overall FWC of the membrane K 120, α and β, the FWCs characteristics of its layers A and B, and x, the percentage of the total membrane thickness corresponding to the A layer, is

$$a = \alpha x + \beta(100 - x)/100 \tag{9}$$

whence β can be calculated. From $\mathcal{L}_P$ measurements, it has been estimated that the A layer thickness of the K 150 membrane is y percent (i.e., 54.8%) of the total thickness. Therefore, the overall FWC of this membrane can be calculated by putting eq. (9) in the following form:

$$\text{FWC} = \frac{\alpha y + \beta(100 - y)}{100} \tag{10}$$

Such calculations can be applied to the bound water content BWC and generalized to all the membranes (Table VIII). From these data, the hydration characteristics of the A, B, C, and D structures can be derived for both MG and K systems (Table IX). These determinations admit a schematic character, because for each layer a constant mean porosity instead of a graded porosity is assumed. However, they show unambiguously, in agreement with a previous paper,[2] that a gap in bound water content exists between the B, C, and D structure types which are sitting during the leaching step in membrane preparation and A structure type which takes form mainly during the evaporation step. Further comments on the relation between hydration characteristics of the A,

TABLE VIII
Values of Free and Bound Water Contents (FWC and BWC, as Defined in Text) in the A, B, C, and D Type Structures for K and MG Membranes at Various Evaporation Times[a]

Membrane	A Structure		B Structure		C Structure		D Structure	
	FWC	BWC	FWC	BWC	FWC	BWC	FWC	BWC
K 240	0.30*	0.40*						
K 150	0.16	0.22	0.29	0.38				
K 120	0.01	0.02	0.61*	0.79*				
K 90			0.46	0.59	0.28	0.23		
K 60			0.20	0.26	0.66*	0.55*		
K 30			0.08	0.11	0.73	0.61	0.15	0.09
K 2			0.03	0.04	0.56	0.47	0.51*	0.30*
MG 240	0.38*	0.35*						
MG 150	0.12	0.11	0.46	0.37				
MG 120	0.03	0.02	0.61*	0.50*				
MG 90			0.63	0.51	0.11	0.01		
MG 60			0.56	0.46	0.30	0.07		
MG 30			0.44	0.36	0.67	0.17		
MG 2			0.33	0.27	1.01*	0.25*		

[a] The basis values, such as these relating to membranes K 240 and K 120 in the calculations given for the membrane K 150, are marked by an asterisk.

TABLE IX
Hydration Characteristics of Structures A, B, C, and D of K and MG Membranes

Type of structure	K Membranes		MG Membranes	
	Free water, g per dry CA g	Bound water, g per dry CA g	Free water, g per dry CA g	Bound water, g per dry CA g
A	0.30	0.40	0.38	0.35
B	0.64	0.83	0.66	0.54
C	0.96	0.80	2.02	0.50
D	1.39	0.82	—	—

B, C, and D structures and membrane preparation conditions will be presented in another paper.

CONCLUSIONS

The present paper provides relationships between transport properties and membrane morphology and hydration in the case of Loeb-type membranes which were prepared under different evaporation times and which exhibit strong structure differences from one to another.

For homogeneous membranes, transport properties are described using the linear relations of thermodynamics of irreversible processes. Interesting relationships have been established between (i) the specific coefficients $\mathcal{L}_P$ and $\mathcal{L}_\pi$ and the amount of capillary water per gram of dry cellulose acetate, and (ii) the specific coefficient $\mathcal{L}_{P\pi}$ and the amount of bound water. These correlations allowed us to describe at a molecular level the pressure dependence of hyperfiltration membrane performance.[17,18] For multilayer membranes, use in an appropriate way of Darcy's law permits correlation between the hydraulic permeability values and the relative extent of four structures A, B, C, and D, as evidenced by electron micrographs. Such an approach provides the values of the specific hydraulic permeability of each type of structure, characterized by strong differences from one to another. In addition, the comparison between these values and hydration data improves the description of the structures A, B, C, and D by determining their hydration intrinsic characteristics. Finally, some experimental results are given, which seem to provide arguments in favor of the suitability of nonequilibrium thermodynamic equations for describing transport properties of such membranes.

The authors would like to thank Professor K. S. Spiegler for stimulating discussions and for some technical data concerning the design of the "concentration clamp" apparatus. This work was supported in part by Contract Action Thématique Programmée Surfaces Solides Complexes No. 2201 from the Centre National de la Recherche Scientifique and by Contract No. 75-7-0175 from the Délégation Générale à la Recherche Scientifique et Technique.

Nomenclature

The superscripts single prime and double prime distinguish between the values corresponding to both the compartments of the transport cell. (For example, c'_s denotes the saline concentration applied to one side of the membrane, c''_s denotes that applied to the other side.)

The subscripts i, j, and k refer, in the model of a multilayer membrane, to the upper, middle, and lower layer, respectively.

c_S	solute concentration in solution, mole/cm^3
e	membrane (or layer) thickness, cm
J_W	water flux, mole/cm^2-sec
J_S	solute flux, mole/cm^2-sec
J_V	volume flux, cm/sec
J_D	chemical flux, cm/sec
L_W, L_{WS}, L_{SW}, L_S	phenomenological coefficients, mole^2/cm^5-atm-sec

$l_P, l_{P\pi}, l_{\pi P}, l_\pi$	transport coefficients, cm/sec-atm
$\mathcal{L}_P, \mathcal{L}_{P\pi}, \mathcal{L}_\pi$	specific transport coefficients, cm^2/sec-atm
P	pressure, atm
P''	atmospheric pressure, atm
$\overline{V}_W$	partial molar volume of water, cm^3/mole
$\overline{V}_S$	partial molar volume of solute, cm^3/mole
ΔP	pressure difference, $P = P' - P''$, atm
$\Delta\pi$	osmotic pressure difference, $\Delta\pi = \pi' - \pi''$, atm
μ_W, μ_S	chemical potentials of water and solute, respectively, cm^3-atm/mole
π	osmotic pressure, atm
σ	reflection coefficient, defined as $-l_{P\pi}/l_P$

References

1. J. Vinit, J. L. Halary, C. Noël, and L. Monnerie, *Eur. Polym. J.*, **11**, 71 (1975).
2. C. Lemoyne, C. Friedrich, J. L. Halary, C. Noël, and L. Monnerie, *J. Appl. Polym. Sci.*, to be published.
3. C. Noël and L. Monnerie, XXIVth International Congress I.U.P.A.C., Symposium on Macromolecules, Jerusalem, 5, 1975, p. 347.
4. S. Loeb and S. Sourirajan, *Adv. Chem. Ser.*, **38**, 117 (1962).
5. Centre National de la Recherche Scientifique, A.T.P. Surfaces Solides Complexes, Final Report of Contract No. 2201, Paris, 1971.
6. D. A. Zelman, J. C. T. Kwak, J. Leibovitz, and K. S. Spiegler, in *Biological Aspects of Electrochemistry*, G. Milazzo, Ed., Birkhäuser Verlag, Basel, 1972, p. 679.
7. H. E. Grethlein, *Desalination*, **16**, 45 (1973).
8. P. I. Lee, Ph.D. thesis, Michigan State University, 1975.
9. J. W. Lorimer, E. I. Boterenbrood, and J. J. Hermans, *Discuss. Faraday Soc.*, **21**, 141 (1956).
10. O. Kedem and A. Katchalsky, *Biochem. Biophys. Acta*, **27**, 229 (1958).
11. R. Schlögl, in *Stofftransport durch Membranen*, D. Steinkopff, Ed., Verlag, Darmstadt, 1964, p. 43.
12. W. Pusch, *Desalination*, **16**, 65 (1975).
13. G. Boari, C. Merli, G. Mossa, and R. Passino, *Desalination*, **16**, 271 (1975).
14. A. J. Staverman, *Rec. Trav. Chim. Pays-Bas*, **70**, 344 (1951).
15. W. Banks and A. Sharples, *J. Appl. Chem.*, **16**, 28 (1966).
16. C. Lemoyne, Thèse de Docteur-Ingénieur, Université Pierre et Marie Curie, Paris, 1976.
17. J. L. Halary, C. Noël, and L. Monnerie, *CR Acad. Sci. Paris, C*, **286**, 689 (1978).
18. B. Grochalski, J. L. Halary, C. Noël, and L. Monnerie, *CR Acad. Sci. Paris, C*, **287**, 491 (1978).
19. J. L. Halary, C. Noël, and L. Monnerie, *Desalination*, **13**, 251 (1973).
20. H. Strathmann, K. Kock, P. Amar, and R. W. Baker, *Desalination*, **16**, 179 (1975).

Received July 7, 1977
Revised January 8, 1979